Periodica Polytechnica Civil Engineering, 70(3), pp. 817–829, 2026

Study on Composite Support Technology of Micropile and Bored Pile Frame for Foundation Pits in Soil-Rock Strata

Heng Ma[1,2], Xiao Feng[3*], Shucai Li[1], Zhenzhong Shi[3], Xiaowei Cao[4], Zhiming Li[4]

[1] Institute of Geotechnical and Underground Engineering, Shandong University, Jinan 250061, China
[2] Shanghai Tunnel Engineering & Rail Transit Design and Research institute, Shanghai 200235, China
[3] School of Transportation Engineering, Shandong Jianzhu University, Jinan 250101, China
[4] Xuzhou Metro Group Co., Ltd., Xuzhou 221000, China
[*] Corresponding author, e-mail: fengxiao19@sdjzu.edu.cn

Received: 14 April 2026, Accepted: 22 June 2026, Published online: 21 July 2026

Abstract

The construction of foundation pits in soil-rock composite strata presents significant challenges due to the mechanical incompatibility between overlying soils and underlying rock masses, often causing abnormal stress redistribution and local instability in conventional pile–anchor support systems. This study proposes a micropile and bored pile frame composite retaining system, wherein reinforced concrete bored piles constitute the primary bidirectional spatial frame and grouted steel micropiles serve as auxiliary members for inter-pile soil retention. The collaborative load-transfer mechanism is analytically characterized through Winkler elastic foundation theory, yielding a stiffness ratio of η = 16.2 between bored piles and micropiles. Field validation was performed at Hou Pantao Village Station on Xuzhou Metro Line 3, wherein full-field strain evolution was monitored using BOTDR distributed optical fiber monitoring throughout staged excavation to a final depth of 17.06 m, with subsequent comparative verification against three-dimensional finite element computations (MIDAS GTS NX). Results demonstrate that: (i) structural deformation concentrates predominantly within the upper 5-m soil layer, with negligible displacement below the rock surface; (ii) micropile peak bending moment migrates downward with excavation, stabilizing near the soil–rock interface; (iii) overburden thickness dominates system response, with a critical threshold at 5 m, beyond which micropile horizontal displacement increased from 5.32 mm to 19.80 mm, matching the field-monitored range (5.70–23.3 mm); (iv) reducing bored pile spacing from 9 m to 4 m decreases maximum micropile displacement by 42.1%, whereas increasing pile diameter yields only local stiffness enhancement without global deformation control.

Keywords

soil-rock composite strata, composite retaining structure, distributed optical fiber monitoring, numerical simulation, deep excavation

1 Introduction

With the rapid economic development of China and the continuous growth in engineering demands, the development of urban underground space and the construction of rail transit networks have been extensively promoted. Consequently, the number of soil–rock composite foundation pits has gradually increased. In such foundation pits, the upper portion within the excavation depth consists of soil layers, while the lower portion comprises rock strata, exhibiting an overall "soft-over-hard" geological characteristic. At present, the design theories and empirical approaches for foundation pits in homogeneous soil or homogeneous rock strata are relatively mature. However, the support design for foundation pits in soil–rock composite strata remains a challenging issue. When traditional pile–strut (or anchor) support systems are applied in soil–rock composite strata, the heterogeneity at the soil–rock interface, significant variations in rock weathering, and the presence of fractures often lead to uneven stress distribution within the support structure. Moreover, it is difficult to maintain local stability of the soil between upper piles, fractured rock zones, and isolated boulders. In recent years, extensive research has been conducted worldwide on support technologies for soil–rock composite foundation pits.

To address the deformation mechanisms and control of deep foundation pits in soil–rock composite strata, numerous studies have been carried out. Zhao et al. [1] studied a Xiamen metro pit in soft-over-hard strata via monitoring and simulation, finding that increasing the diaphragm

Cite this article as: Ma, H., Feng, X., Li, S., Shi, Z., Cao, X., Li, Z. "Study on Composite Support Technology of Micropile and Bored Pile Frame for Foundation Pits in Soil-Rock Strata", Periodica Polytechnica Civil Engineering, 70(3), pp. 817–829, 2026. https://doi.org/10.3311/PPci.44302

wall's rock-socketed ratio effectively reduced deformation, and proposed a hinged top support system for optimization. Zhang et al. [2] used numerical simulation to study overbreak and underbreak in subway stations within interbedded soft–hard interbedded rock, revealing distinct blasting failure mechanisms and proposing asymmetric precision-controlled parameters that improved excavation quality. Sun et al. [3] combined variational mode decomposition and neural networks to predict foundation pit displacement, improving accuracy in complex geological conditions. Guan et al. [4] confirmed millimeter-level 3D deformation monitoring for retaining structures in soil-rock composite pits via close-range photogrammetry. Xu et al. [5], focusing on a deep soil–rock composite foundation pit adjacent to an existing excavation, introduced an axial force servo-controlled support system and revealed the deformation evolution law of the retaining structure under asymmetric loading, showing that servo control effectively restrains lateral displacement toward the adjacent pit. Zhang et al. [6], based on an ultra-deep soil–rock composite foundation pit in Qingdao, found through monitoring and numerical analysis that the conventional design method treating rock mass as equivalent soil fails to reasonably reflect structural effects of rock mass. They proposed staged calculation and differentiated parameter selection to avoid excessive support. Li et al. [7], investigating a 40 m deep foundation pit in a composite rock–soil stratum in Guangzhou, systematically analyzed the deformation characteristics of a suspended diaphragm wall and reported that the maximum lateral displacement was significantly smaller than conventional empirical values, with anchor prestress identified as the key control parameter. Zhou et al. [8] introduced a physics-informed machine learning approach for deformation prediction of support structures in heterogeneous soil layers, embedding mechanical governing equations into neural networks to achieve efficient and high-precision prediction in soil–rock composite strata. Nicotera and Russo [9] found through long-term monitoring of a deep foundation pit in volcanic pyroclastic soil–soft rock composite strata that deformation during the main excavation stage was effectively controlled, whereas groundwater control failure during subsequent tunnel construction induced significant additional settlement. Tabaroei et al. [10] simulated the Texas A&M excavation case, compared numerical results with field measurements, and investigated the influence of ground anchor arrangement on wall horizontal displacement and surface settlement. Movahedi Rad [11] employed reliability-based limit analysis to determine the ultimate lateral capacity of free-head and fixed-head long piles, introducing an uncertain bound on the complementary strain energy of residual forces to control the plastic behavior of the structure. For the numerical simulation method of deep foundation pit engineering, Szepesházi and Móczár [12] carried out two-dimensional and three-dimensional numerical inversion analysis on two deep foundation pit cases in Budapest, Hungary, and compared the numerical simulation results with field measured data, confirming that the three-dimensional numerical model can provide more accurate calculation results than the two-dimensional model. In the field of optimization design of pile foundation and geotechnical supporting structures, Mohavedi Rad and Ibrahim [13] proposed an optimal plastic analysis and reliability design method for pile foundations based on shakedown theory, and found through finite element analysis that this method can achieve significant material savings compared with the conventional elastic design method. Atenov and Bekbasarov [14] proposed vertical bearing capacity formulas for precast piles with conical and spherical enlarged heads using finite-discrete element analysis. Kaveh et al. [15] compared 11 metaheuristic algorithms for reinforced concrete cantilever retaining walls, finding VPS and WEO optimal for cost and convergence. Aiming at the pile-soil interaction mechanism of supporting structures, Lődör and Móczár [16] developed a 3D finite element model for pile-soil interaction, accurately predicting settlement and bearing capacity of improved foundations, validated by Budapest field measurements. Haouari and Bouafia [17] combined centrifuge tests and ABAQUS to evaluate sand density and pile depth effects on lateral pile response, proposing a nonlinear pile-soil interaction method. For the mechanical parameter determination of rock and soil mass in composite strata, Vásárhelyi and Kovács [18] analyzed measured data to identify how lithology, weathering, and structural planes affect rock mass parameters.

Current studies mainly focus on pile–anchor or anchor-shotcrete support systems, in which the vertical retaining members are typically limited to a single type, such as bored piles or micropiles, making it difficult to accommodate the high variability of soil–rock composite strata. Meanwhile, when anchor cables (or rods) are adopted as horizontal members, it is challenging to establish a reliable spatial load-bearing system, and issues such as encroachment on adjacent property and the formation of underground obstacles often arise. Therefore, it is necessary to explore and validate new composite support technologies.

Based on the existing literature, this study proposes a novel micropile–bored pile frame composite support system. The foundation pit of Hou Pantao Village Station, Phase II of Metro Line 3 in Xuzhou, was selected as the engineering background. Distributed optical fiber sensing was implemented in the field to obtain the working performance of the support system and soil deformation during excavation. Furthermore, finite element modeling and parametric analysis were conducted using MIDAS GTS NX to investigate the effects of cross-sectional dimensions and spacing of bored piles and micropiles, as well as soil parameters, on the support performance. The findings of this study can provide theoretical reference for similar engineering projects.

2 Micropile–bored pile frame composite support system

2.1 Composition and design of the support system

To address the large stiffness contrast between overlying soils and underlying rocks in soil–rock composite strata, the limitations of conventional support systems, and the difficulty in maintaining local soil stability between piles, this study proposes a micropile–bored pile frame composite support system. The system comprises bored reinforced concrete piles, micropiles, a reinforced concrete crown beam at the top of the excavation, internal struts, and steel struts with wales at various levels. The configuration of the structural components is illustrated in Fig. 1.

The primary load-bearing structure is a bidirectional integral frame system, wherein reinforced concrete bored piles serve as vertical members, and crown beams or wales combined with internal struts at each level function as horizontal members. Micropiles, formed by inserting seamless steel pipes into predrilled holes and grouting them in place between adjacent bored piles, act as auxiliary load-bearing members to ensure local soil stability between the piles.

The proposed structure forms a spatially coordinated support system through the synergistic interaction between the bidirectional integral frame and the micropiles. Through the connections at the crown beams and wales, a portion of the earth pressure is resisted by the frame support system, whereas the remainder is transferred to the micropiles. This load-sharing mechanism yields a more uniform stress distribution within the overall structure, enabling effective control of rock and soil mass deformation and thus enhancing the safety performance of foundation pit engineering.

2.2 Synergistic working mechanism analysis

The load transfer mechanism of the micropile–bored pile frame composite support system can be simplified as a dual-stiffness retaining structure interacting with stratified ground. To quantify the load-sharing behavior between bored piles and micropiles, a simplified analytical model based on the Winkler elastic foundation beam theory is established.

Assuming the crown beam/wale as a rigid connecting element, the lateral earth pressure acting on the retaining structure is redistributed according to the relative stiffness of bored piles and micropiles. The relative stiffness ratio η is defined as:

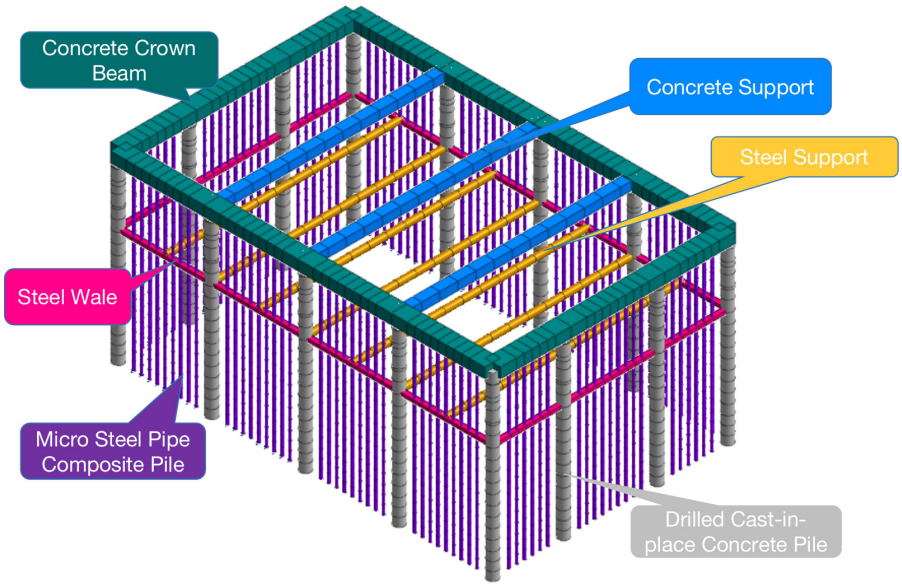

Fig. 1 Micropile–bored pile frame composite support system

$$\eta = \frac{k_{bp}}{k_{mp}} \tag{1}$$

where: k_{bp} and k_{mp} are the lateral stiffness coefficients of the bored pile and micropile, respectively.

The lateral stiffness coefficients can be expressed as:

$$k = \frac{3EI}{h^3 \times S} \tag{2}$$

where: E is the elastic modulus, I is the moment of inertia, h is the free length above the excavation surface, and S is the pile spacing.

For a bored pile with diameter D_{bp} = 900 mm, spacing S_{bp} = 9 m, elastic modulus E_{bp} = 3.15 × 104 MPa, and free depth h = 8.5 m, substituting these values into Eq. (2) yields k_{bp} = 550.38 kN/m^2. For a micropile with diameter D_{mp} = 152 − 2 × 6 = 140 mm, spacing S_{mp} = 0.75 m, elastic modulus E_{mp} = 2.00 × 105 MPa, and free depth h = 8.5 m, substituting these values into Eq. (2) yields k_{mp} = 9.37 kN/m^2.

Based on existing research, the frame action significantly enhances the stiffness of micropiles far more than that of bored piles. Due to the inherently large stiffness of bored piles, the frame action improves their lateral stiffness by approximately 2.0–3.5 times [19]; in this paper, the median value of 2.75 is adopted. In contrast, micropiles possess minimal individual pile stiffness, and through the combined effect of crown beams and wales, their effective stiffness can be increased by 5.0–15.0 times [20, 21]; in this paper, the median value of 10.0 is adopted. Substituting the enhanced stiffness values of bored piles and micropiles into Eq. (1) yields a relative stiffness ratio of 16.2 between the bored pile and the micropile.

This indicates that the bored pile frame provides the primary global resistance, while micropiles contribute to local soil retention between piles. However, considering the composite action through the crown beam, the effective stiffness of the micropile-reinforced soil zone increases significantly.

3 Field experimental study

3.1 Engineering background

The main structure of Hou Pantao Village Station on Phase II of Xuzhou Metro Line 3 is a reinforced concrete double-layer, double-span box frame structure. It is an underground two-level island-platform station with an 11 m-wide platform, and shield launching shafts are arranged at both ends. The embedment depth of the bottom slab at the station centerline is approximately 17.06 m. The center mileage of the station is CK0+250.000 (right line), with a total length of approximately 482.8 m and a width ranging from 19.7 m to 35.0 m.

The foundation pit is supported by the proposed micropile–bored pile frame composite support system. The reinforced concrete bored piles have a diameter of 900 mm and a spacing of 9 m, while the micropiles have a diameter of 152 mm and a spacing of 750 mm. Two levels of internal supports are arranged along the excavation depth. The first level comprises reinforced concrete struts with a cross-sectional dimension of 800 × 900 mm, and the second level comprises steel pipe struts with a diameter of 609 mm. The reinforced concrete crown beam has a cross-sectional dimension of 1500 × 1000 mm, and the steel wales are composed of double 45C I-shaped steel sections. The cross-sectional view of the foundation pit support system is shown in Fig. 2.

3.2 Experimental scheme

To investigate the working performance of the micropile–bored pile frame composite support system and the deformation characteristics of the surrounding soil during excavation, several micropiles on both the north and south sides of the foundation pit, and the adjacent rock–soil mass near the retaining structure on the south side, were selected for instrumentation. Field monitoring was conducted using BOTDR (Brillouin Optical Time Domain Reflectometry) distributed optical fiber sensing technology. The layout of the monitoring points is shown in Fig. 3.

The BOTDR distributed optical fiber sensing technique utilizes the linear relationship between the Brillouin frequency shift and the variations in strain and temperature of the optical fiber to measure strain or temperature. The axial strain of the optical fiber bonded to or embedded within the monitored object can be calculated according to Eq. (3):

$$v_B(\varepsilon, T) = v_B(0, T_0) + \frac{\partial v_B(\varepsilon)}{\partial \varepsilon} \times \varepsilon + \frac{\partial v_B(T)}{\partial T} \times (T - T_0) \tag{3}$$

where: $v_B(\varepsilon, T)$ represents the Brillouin frequency shift of the optical fiber under environmental strain ε and temperature T; $v_B(0, T)$ denotes the Brillouin frequency shift of the optical fiber at zero strain and temperature T; $\partial v_B(\varepsilon)/\partial \varepsilon$ and $\partial v_B(T)/\partial T$ are the strain and temperature coefficients related to the type of optical fiber, respectively.

In this test, optical fiber sensors were installed along micropiles and in adjacent rock–soil boreholes to monitor

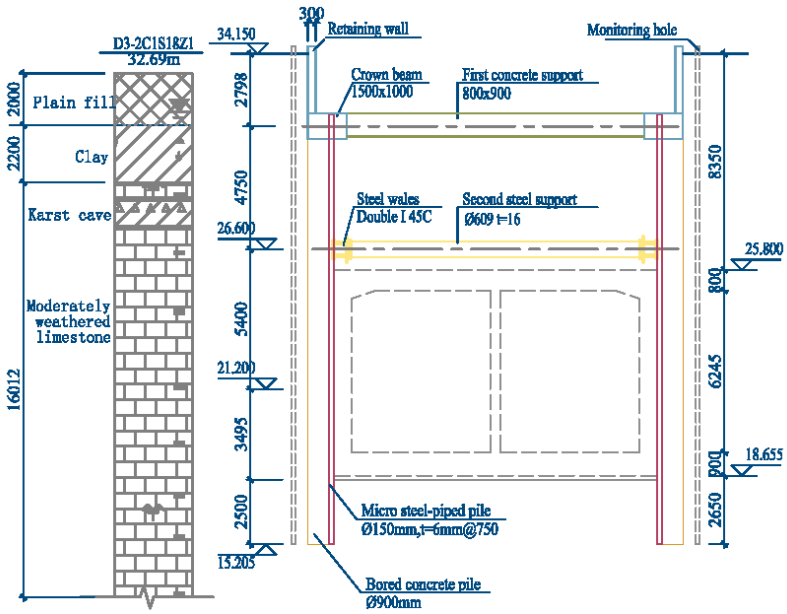

Fig. 2 Design of the retaining structure for Hou Pantao Village Station Foundation Pit

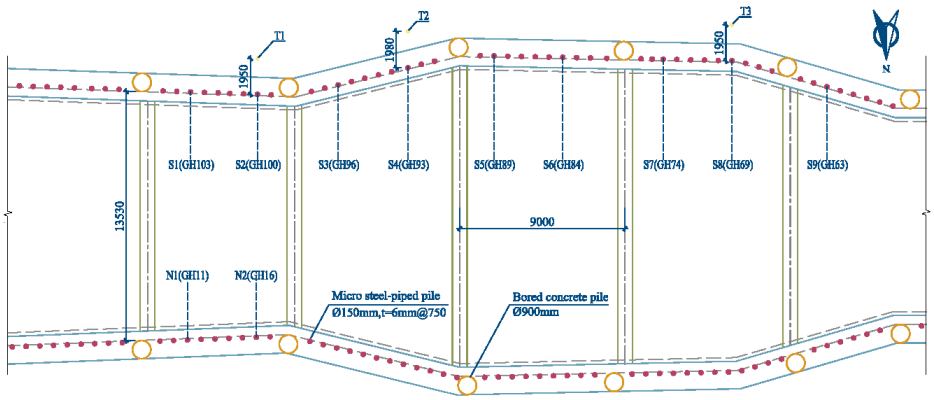

Fig. 3 Plan layout of monitoring points

deformation during excavation. Pile internal forces were derived from measured strains using an AV6419 BOTDR analyzer (CETC) (accuracy: ±2 με, dynamic range: 20 dB, scanning range: 10.0–13.0 GHz).

Optical fibers were installed within micropiles in a U-shaped layout, secured to the inner wall via pre-drilled holes and protected by epoxy-coated steel cables and metal sleeves at the crown beam. After fusion-splicing was completed, the AV6419 analyzer verified connectivity and collected initial strain data post-calibration. The test layout of micropiles is shown in Fig. 4.

Three rock–soil monitoring boreholes were arranged at a horizontal distance of 2 m from micropiles GH100, GH93, and GH69 on the south side. For rock–soil monitoring, boreholes with a diameter of 125 mm and a depth of 16 m were drilled. The optical fiber sensor was fixed to a weighted guide hammer and slowly lowered into the

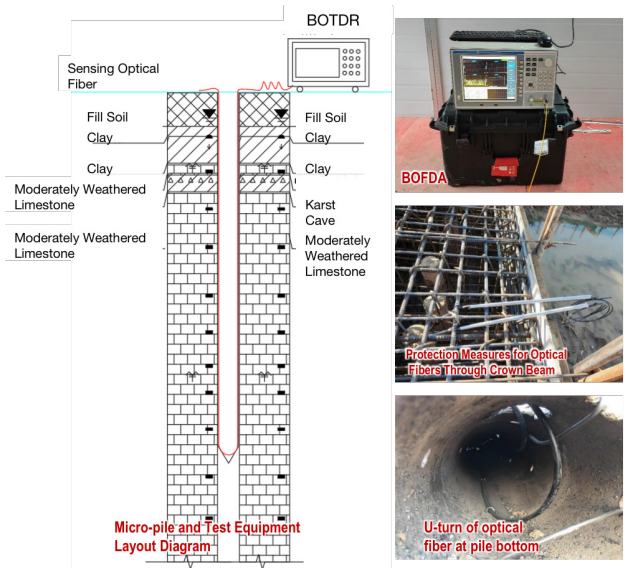

Fig. 4 Test layout of micropiles

borehole until the sensor reached the bottom. The sensing fiber was arranged in a "U"-shaped configuration. Plain concrete was then poured into the borehole to ensure close contact between the fiber sensor and the surrounding rock–soil mass, thereby achieving effective deformation coupling. Similarly, a 5 m length of sensing fiber was reserved at the borehole opening for subsequent connection.

Excavation of the foundation pit supported by micropiles at Hou Pantao Village Station commenced on November 30, 2021. In accordance with the actual construction progress, a total of ten rounds of optical fiber data acquisition were completed.

3.3 Test results

The strain results measured along the micropiles at each monitoring point were converted into bending moments according to Eq. (4):

$$M = E_{mp} I_{mp} \frac{\varepsilon_{test}}{D_{mp}/2} \tag{4}$$

where: M is the calculated bending moment; $E_{mp}I_{mp}$ is the flexural rigidity of the micropiles; ε_{test} is the strain value of the micropiles measured by the optical fiber; D_{mp} is the diameter of the micropiles.

The strain distribution in micropiles is shown in Fig. 5.

As excavation progressed, the bending moment of the micropiles exhibited an increasing trend. Taking Fig. 5(f), which presents the bending moment distribution of micropile GH93, as an example, the strain in the micropiles gradually increased as excavation proceeded. When the excavation depth reached 9.3 m below the bottom of the crown beam, the strain attained its maximum value, with the peak located approximately 2 m below the crown beam bottom. The strata at this depth comprise, in sequence, clay, moderately weathered limestone, a karst cave, and moderately weathered limestone. Due to the significant lithological variation and relatively loose rock–soil mass prone to collapse, a relatively large bending moment developed in the micropile steel pipe pile.

After the diaphragm wall was concreted, the strain peak decreased, indicating that the steel pipe struts effectively reduced micropile deformation. Below 7 m from the crown beam bottom, the bending moment values of the micropiles were relatively small. This can be attributed to the presence of moderately weathered limestone at this depth, which exhibits good self-supporting capacity and is less prone to collapse. In addition, the installation of the second-level steel strut and the diaphragm wall further reduced micropile deformation in this zone. The underlying bedrock at the site is Ordovician limestone, located at the core and eastern limb of a syncline, dipping toward N128°W with a dip angle of approximately 35°. Consequently, the bending moment values of micropiles GH11 and GH16 on the north side are smaller than those of GH103 and south GH100 on the south side at corresponding positions.

The peak bending moment of the micropiles gradually shifted downward with increasing excavation depth, eventually stabilizing at approximately 2–3 m below the crown beam bottom. This location corresponds to the transitional zone of moderately weathered limestone–karst cave–moderately weathered limestone, which is characterized by significant lithological variability and relatively loose ground conditions. Combined with the overlying miscellaneous fill, which is prone to collapse, the earth pressure acting on the micropiles at this position reaches its maximum. Below 7 m from the crown beam bottom, the stratum mainly comprises relatively intact moderately weathered limestone, which exhibits good self-stability and contributes to slope stability. Moreover, steel pipe struts were installed promptly after excavation, resulting in relatively low rock pressure and bending moments in the micropiles below this depth.

The monitoring results for the rock–soil mass are shown in Fig. 6. Based on the strain distribution in monitoring borehole T1, when the excavation depth was 0–5.8 m, the strain peak at micropile GH100 (adjacent to this borehole) occurred at a depth of 1.5 m in a clay layer with relatively good self-supporting capacity. At this stage, the maximum rock–soil strain reached 379 με. When the excavation depth increased to 9.3 m, the strain peak shifted downward and stabilized at approximately 2.8 m below the crown beam bottom, reaching a maximum strain of 431 με. This depth corresponds to the transitional zone of clay–moderately weathered limestone–karst cave–moderately weathered limestone, where complex lithology and strong variability result in a high susceptibility to collapse and consequently larger ground deformation.

A comparative analysis between the rock–soil strain monitored at T2 and the strain in micropile GH93 located on the same alignment indicates that, at the same excavation depth, the strain in the rock–soil mass was smaller than that of the micropile. After the installation of steel pipe struts, creep deformation occurred in the rock–soil mass, and the reduction in rock–soil strain was smaller than that in the micropile.

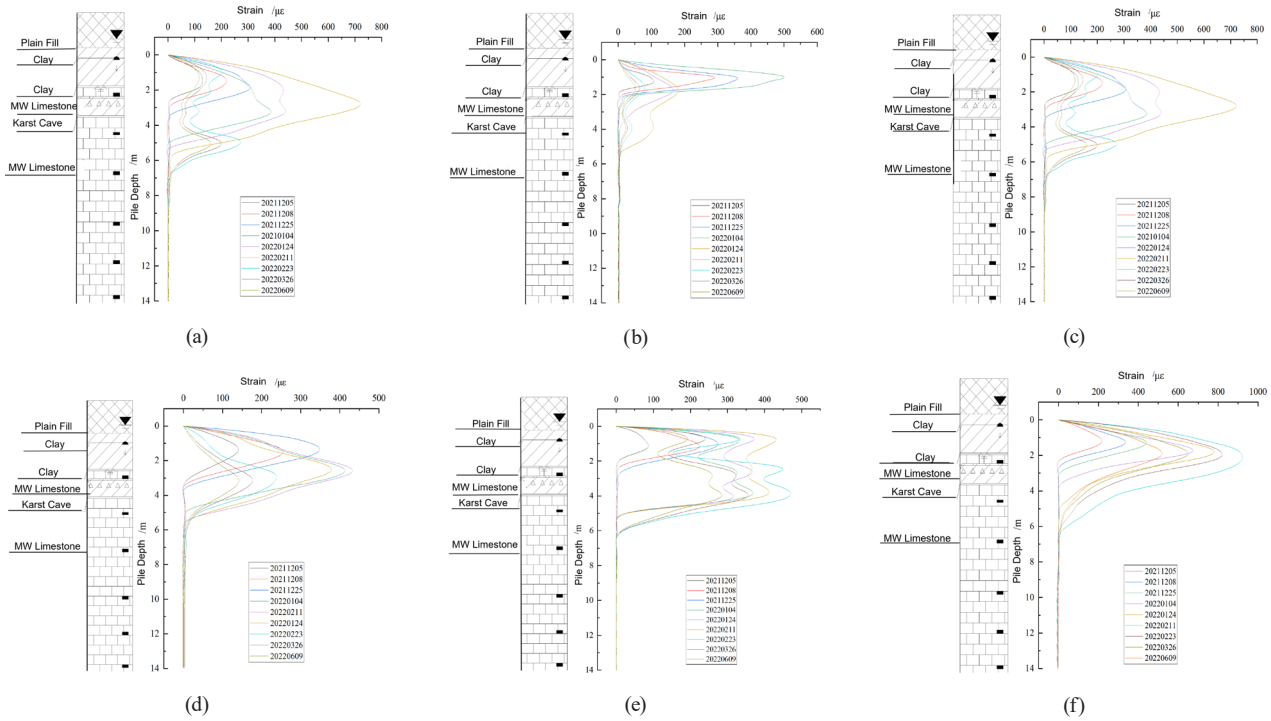

Fig. 5 Strain distribution in micropiles: (a) GH11, (b) GH16, (c) GH103, (d) GH100, (e) GH 96, (f) GH93

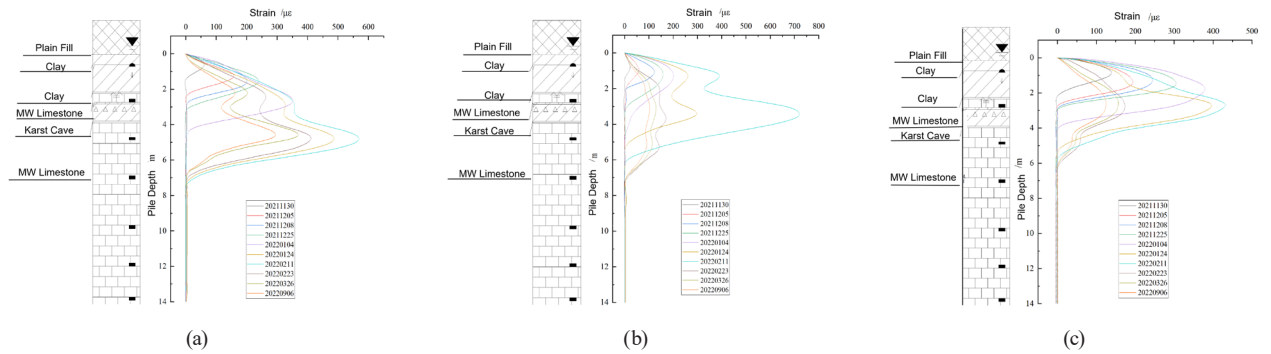

Fig. 6 Monitoring results of rock–soil boreholes: (a) monitoring point T1, (b) monitoring point T2, (c) monitoring point T3

4 Parameter analysis

4.1 Establishment and verification of the finite element model

To further investigate the effects of different design parameters of the micropile–bored pile frame composite support system on system performance, a three-dimensional numerical model was established using MIDAS GTS NX to simulate the excavation process of the soil–rock composite foundation pit. The following assumptions were adopted during modeling:

1. According to the geological profile and borehole log data within the simulation area, strata with minor undulations were simplified as horizontal layers;
2. The model range approximately covered three bored piles, and the plan-view corner effects of the retaining structure were not considered;
3. Horizontal displacements were restrained at the lateral boundaries of the model, while vertical displacement was restrained at the bottom boundary;
4. Key construction stages were considered in the simulation, while secondary construction procedures were omitted.

The overall model dimensions are 75 m × 27 m × 36 m. The global model and the detailed support structure model are shown in Fig. 7.

To accurately represent the mechanical behavior of the rock–soil mass, the Hardening Soil (HS) constitutive model was adopted for miscellaneous fill and clay, while a jointed rock constitutive model was employed for moderately weathered limestone. The calculation parameters were determined according to the geotechnical

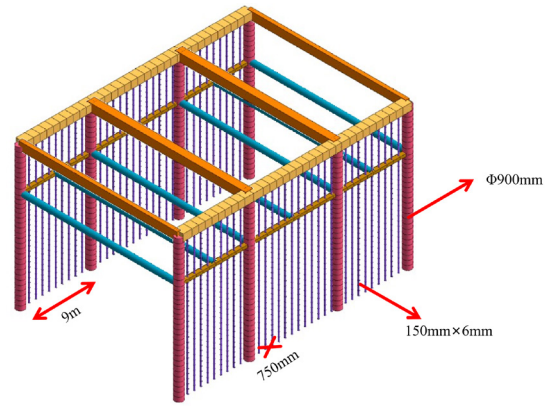

(a)

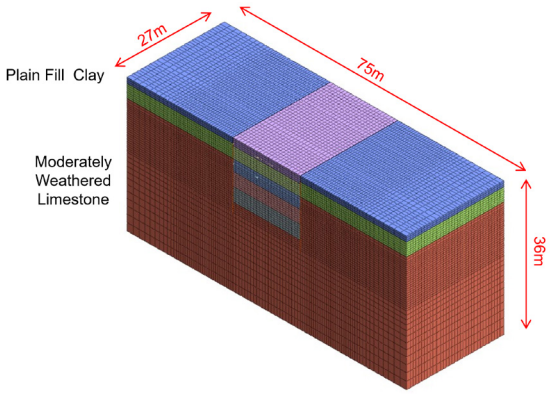

(b)

Fig. 7 (a) Global finite element model and (b) support structure model

investigation report of the project. The specific parameters for the rock–soil mass are listed in Tables 1 and 2.

The supporting structures were modeled as linear elastic materials. The material parameters of structural components are provided in Table 3, and the element types and geometric characteristics are summarized in Table 4.

According to the actual construction sequence on site, the entire process of support installation and staged excavation was simulated. The construction steps in the numerical model were defined as follows:

(1) Initial in-situ stress analysis with displacement reset to zero; (2) Installation of bored piles and micropiles; (3) Excavation of the soil layer to a depth of 1.95 m, followed by construction of the crown beam and the first-level reinforced concrete strut; (4) Further excavation of 3.0 m; (5) Additional excavation of 3.0 m; (6) Further excavation of 3.5 m; (7) Continued excavation of 3.7 m down to the final pit bottom.

To validate the numerical model for simulating support structures and excavation sequences, the

Table 3 Calculation parameters of materials for foundation pit support components

Materials	Volume weight (kN/m^3)	Poisson ratio	Elasticity modulus (MPa)
C35 concrete	25	0.2	3.15×10^4
C30 concrete	25	0.2	3.00×10^4
Q235 steel	78	0.3	2.00×10^5

Table 1 Calculation parameters table of plain fill soil and clay

Parameter	Depth h (m)	Volume weight γ (kN/m^3)	Apparent cohesion c (kPa)	Internal friction angle φ (°)	E_{50} (kPa)	E_{oed} (kPa)	E_{ur} (kPa)
Filling	1.31	18	8.0	20.0	5850	4500	25650
Clay	3.70	19	43.5	9.9	8190	6300	35910

Table 2 Rock mass calculation parameters table

Parameter	Volume weight	Elasticity modulus		Poisson ratio		Shear elasticity		Number of joint layers	Dip angle	Joint element Apparent cohesion	Joint element Internal friction angle
Portion and unit	γ (kN/m^3)	E_1 (MPa)	E_2 (MPa)	μ_{12}/μ_{13}	μ_{23}	G_{12}/G_{13} (MPa)	G_{23} (MPa)	n	θ_{dip} (°)	c_{joint} (kPa)	φ_{joint} (°)
Value	26.8	18000	14062.5	0.28	0.28	7031.25	4123.9	1	35	200	35

Table 4 Types and geometric characteristics of foundation pit support component units

Structural style	Unit type	Material property	Geometric features of cross-section
Cast-in-place pile	Beam	C35	Diameter 900 mm, Pile length 16.7 m
Micropile	Beam	Q235	External diameter 152 mm, wall thickness 6 mm, pile length 16.7 m
Concrete support	Beam	C30	800 × 900 mm
Steel support	Beam	Q235	External diameter 609 mm, wall thickness 16 mm
Top beam	Beam	C30	1500 × 1000mm
Encircling purlin	Beam	Q235	Double 45C I-beam

finite-element-calculated bending moments of the micropiles were extracted and comprehensively compared with field measurements at multiple monitoring points (Table 5). The favorable agreement confirms the model's reasonable accuracy.

Based on the validated model, parametric analyses were subsequently performed by varying the thickness of the overlying soil layer, soil mechanical properties, spacing of bored piles, and the spacing of micropiles. These analyses aim to clarify the influence of different soil–rock strata conditions and support design parameters on the performance of the composite support system.

4.2 Different thicknesses of overlying soil layers

The original overburden above the foundation pit consisted of plain fill and clay, with thicknesses of 1.45 m and 3.5 m, respectively. In this section, the total overburden thickness was varied by adjusting the thickness of the clay layer. The clay thickness was set to 1.55 m, 2.55 m, 3.55 m, 4.55 m, 5.55 m, and 6.55 m in the respective numerical models. When one parameter was modified, all other parameters were maintained at their original design values; the same principle applies hereafter and will not be repeated. The horizontal displacement curves of the micropiles at the end of excavation, as computed by FE analysis, are presented in Fig. 8, and the corresponding maximum values of horizontal soil displacement, ground surface settlement, and horizontal displacement of the micropiles are summarized in Fig. 9.

The displacement curves of both the soil mass and the micropiles indicate that, for soil–rock composite foundation pits, the thickness of the overlying soil layer has a significant influence on pile deformation. When the soil thickness increases to approximately 5.0 m, both the horizontal displacement of the soil and that of the micropiles increase rapidly. This suggests that the restraining effect of the reserved rock mass at the pit bottom on the supporting piles becomes more pronounced in foundation pits with thicker overburden. Meanwhile, the location of the maximum horizontal displacement of the piles exhibits a gradual downward shift.

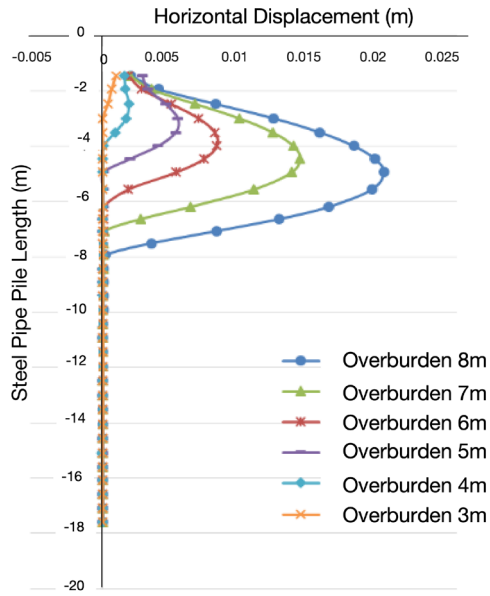

Fig. 8 Micropile displacement vs. overburden thickness

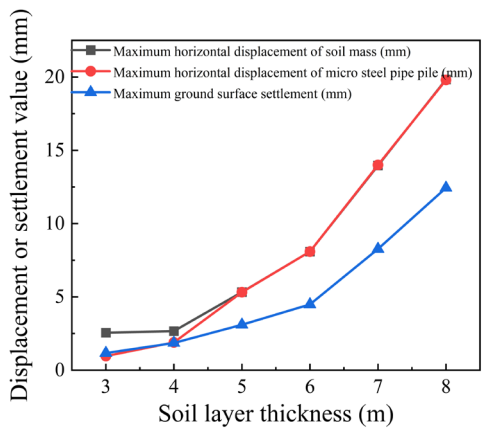

Fig. 9 Soil and pile displacement vs. overburden thickness

As the overburden thickness reaches about 5.0 m, the ground surface settlement adjacent to the pit increases sharply. When the overburden thickness ranges from 5 m to 8 m, the horizontal displacement of the micropiles increases from 5.32 mm to 19.80 mm, which is close to the monitored displacement range of 5.7 mm to 23.3 mm (Table 6). Considering the existence of large karst cavities in the rock mass, possible construction overloading, and local failure of individual micropiles, the measured values are slightly greater than the numerical predictions.

Table 5 Comparison of calculated and measured maximum bending moments of micropiles

Monitoring point	Field-measured M_{max} (kN m)	FE-computed M_{max} (kN m)	Relative error
GH 103	11.27	10.83	−3.9%
GH 100	6.74	7.08	5.1%
GH 96	7.30	7.66	4.9%
GH 93	14.62	15.34	4.9%

Note: Relative error = (FE-computed M_{max} - Field-measured M_{max})/Field-measured M_{max}

Table 6 Maximum monitored horizontal displacement of the micropiles

Monitoring point	GH103	GH100	GH96	GH93	GH89	GH84	GH74	GH69	GH63
Maximum horizontal displacement (mm)	21.1	11.7	5.7	23.3	20.6	13.0	19.0	11.7	17.2

4.3 Influence of cohesion of the overburden soil

The deformation of the retaining structure and the surrounding ground surface in soil–rock composite foundation pits is strongly influenced by the properties of the overlying soil. Cohesion (c) is an important parameter for evaluating soil quality. By varying the cohesion of the overlying clay layer, the deformation characteristics of the supporting structure and surrounding strata at the completion of excavation were investigated.

Four simulation schemes were established, in which the cohesion of the overburden soil was set to 0.4, 0.6, 0.8, and 1.0 times the value recommended in the geotechnical investigation report, respectively. The horizontal displacement curves of the micropiles at the end of excavation are shown in Fig. 10. The corresponding maximum values of horizontal soil displacement, ground surface settlement, and horizontal displacement of the micropiles are summarized in Fig. 11.

The results indicate that, for soil–rock composite foundation pits, as the cohesion of the overlying soil decreases, the horizontal displacement of the piles on both sides of the foundation pit and the ground surface settlement gradually increase. The maximum displacement of the micropiles is located at approximately 3.0 m below the ground surface. A comparison between the pile displacement curves and the ground settlement trends shows a certain degree of correlation between horizontal pile displacement and surface settlement.

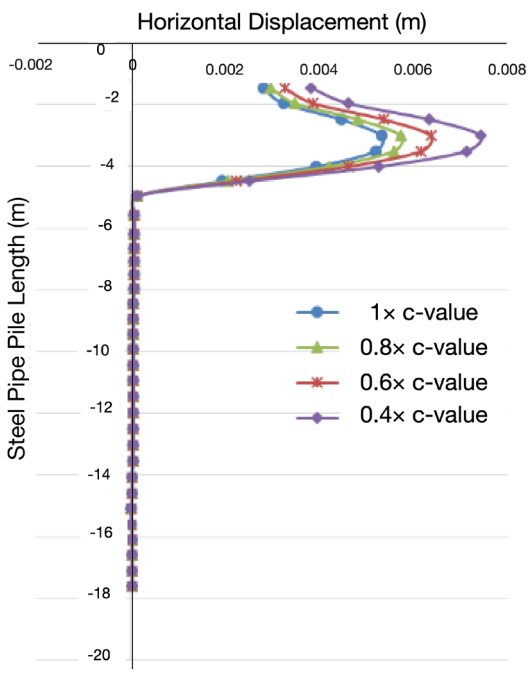

Fig. 10 Horizontal displacement of micropiles vs. soil cohesion

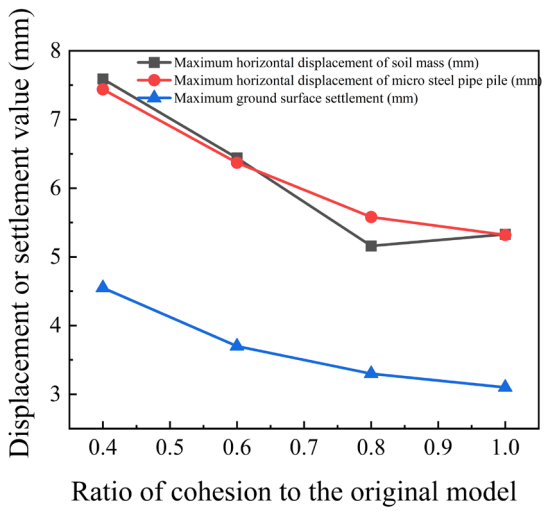

Fig. 11 Soil-pile displacement vs. overburden cohesion

Overall, compared with the influence of overburden thickness, the variation in soil cohesion has a relatively smaller effect on the horizontal displacement of the supporting piles.

4.4 Analysis of design parameters of bored cast-in-place piles

The diameter and spacing of bored cast-in-place piles are core design parameters of the composite retaining system, and their selection plays a crucial role in controlling foundation pit deformation. In this study, numerical models with different pile diameters and spacings were established to investigate their influence on the excavation behavior of soil–rock composite foundation pits and the surrounding ground response.

Numerical models with bored pile diameters of 800 mm, 900 mm, and 1000 mm were developed and analyzed. The horizontal displacement curves of the micropiles and bored piles at the end of excavation are shown in Fig. 12 and Fig. 13, respectively. The maximum values of horizontal soil displacement, ground surface settlement, and horizontal displacement of the micropiles are summarized in Fig. 14.

The displacement curves indicate that, as the diameter of the bored piles increases, the maximum soil displacement and the displacement of the micropiles change only slightly,

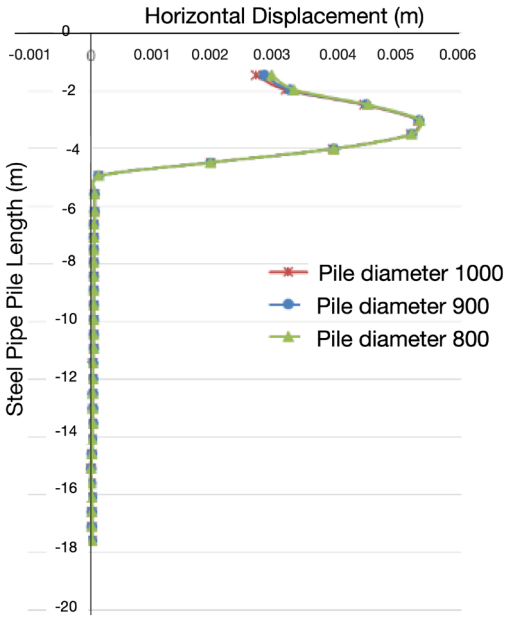

Fig. 12 Micropile displacement vs. bored pile diameter

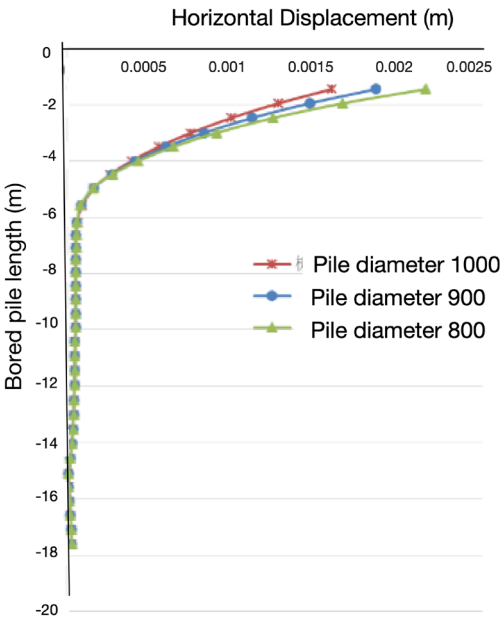

Fig. 13 Bored pile displacement vs. pile diameters

whereas the displacement of the bored piles decreases with increasing pile diameter. Ground surface settlement also decreases as the pile diameter increases. The maximum deformation of the foundation pit generally occurs at the relatively weaker micropiles. Therefore, merely increasing the diameter of the bored piles does not significantly reduce the maximum deformation of the foundation pit.

In addition, models with bored pile spacings of 3.5 m, 4 m, 8 m, and 9 m were established for analysis. The horizontal displacement curves of the micropiles and bored

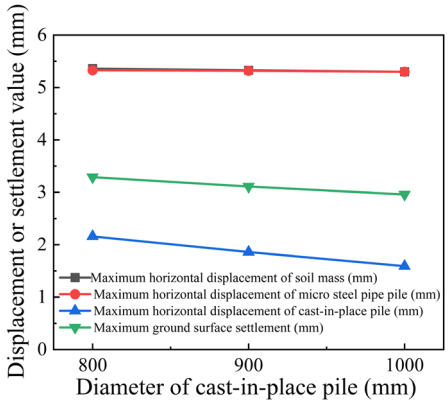

Fig. 14 Soil and pile displacements vs. bored pile diameter

piles at the end of excavation are shown in Figs. 15 and 16, respectively, and the corresponding maximum values are summarized in Fig. 17.

As shown in Fig. 15, reducing the bored pile spacing from 9 m to 4 m decreased the maximum lateral displacement of the micropiles from 5.32 mm to 3.08 mm (a reduction of 42.1%). However, further reduction to 3.5 m yielded only marginal improvement (an additional decrease of 0.1 mm).

Fig. 16 indicates that the displacement of the bored piles decreased significantly with reduced spacing, from 1.86 mm at 9 m spacing to 0.91 mm at 3.5 m spacing. As the spacing approached 3.5–4 m, the bored piles increasingly behaved as a continuous wall; correspondingly, as shown in Fig. 17, the maximum ground surface settlement decreased from 3.11 mm at 9 m spacing to 1.65 mm at 4 m spacing.

Based on the above analysis, reducing the bored pile spacing proves to be an effective measure for controlling

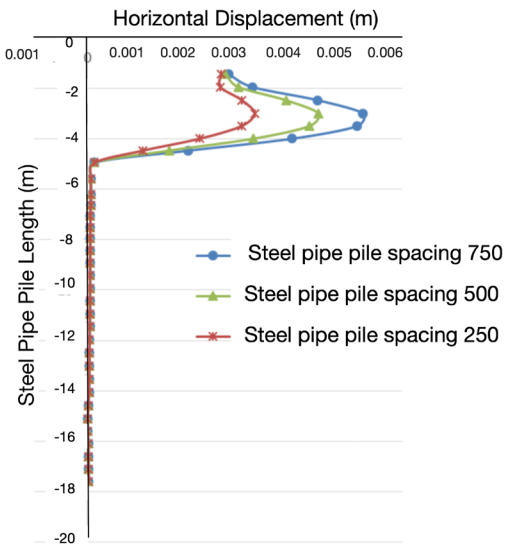

Fig. 15 Micro pile horizontal displacement vs. bored pile spacings

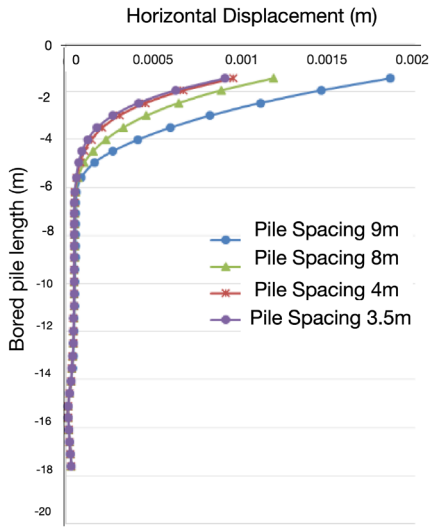

Fig. 16 Bored pile horizontal displacement vs. bored pile spacings

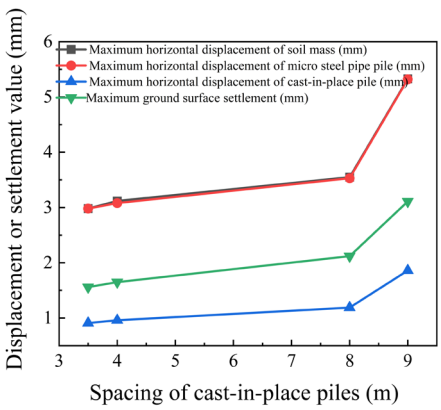

Fig. 17 Soil and pile deformation vs. bored pile spacings

overall excavation deformation, particularly applicable to scenarios with strict deformation limits or overburden thicknesses exceeding 5 m.

5 Conclusions

1. To address foundation pit support challenges in soil–rock composite strata, a micropile–bored pile frame composite system is proposed. Field monitoring and 3D FEM analysis (MIDAS GTS NX) of the Xuzhou Metro Line 3 project investigated the effects of overburden thickness, soil cohesion, and pile design parameters.
2. The composite system forms a spatial frame via bored piles (with crown beams, wales, struts) and micropiles, which enhances stiffness and improves local stability. Field monitoring confirms its effectiveness in soil–rock strata.
3. Deformation is concentrated in the upper soil layer, with minimal rock deformation. Micropile peak bending moment shifts downward with excavation depth. Rock excavation causes limited additional lateral displacement, stabilizing below the rock surface.
4. Parametric analysis shows overburden thickness most significantly increases displacement and settlement, with soil cohesion having less effect. Larger bored pile diameter only reduces its own displacement. Reduced bored pile spacing effectively controls overall deformation. Increasing micropile stiffness or reducing spacing significantly restrains soil displacement and settlement, improving local stability.

Acknowledgement

The authors would like to express their sincere appreciation to the reviewers for their valuable comments and suggestions, which helped improve the quality of the paper.

Funding

The authors gratefully acknowledge the financial support from the National Natural Science Foundation of China (Grant No. 52009075), the Natural Science Foundation of Shandong Province (Grant Nos. ZR2020QE262 and ZR2024ME119), and the Doctoral Research Fund of Shandong Jianzhu University (Grant Number X19018Z).

References

[1] Zhao, J., Tan, Z., Yu, R., Li, Z., Zhang, X., Zhu, P. "Deformation responses of the foundation pit construction of the urban metro station: A case study in Xiamen", Tunnelling and Underground Space Technology, 128, 104662, 2022. https://doi.org/10.1016/j.tust.2022.104662

[2] Zhang, W., Mei, J., Sun, K., Xu, B. "Fine controlled blasting of subsurface excavation for subway stations in soft–hard mixed-medium rock mass", Tunnelling and Underground Space Technology, 158, 106407, 2025. https://doi.org/10.1016/j.tust.2025.106407

[3] Sun, L., Liu, S., Zhang, L., He, K., Yan, X. "Prediction of the displacement in a foundation pit based on neural network model fusion error and variational modal decomposition methods", Measurement, 240, 115534, 2025. https://doi.org/10.1016/j.measurement.2024.115534

[4] Guan, L. L., Chen, Y. G., Liao, R. P. "Accuracy Analysis for 3D Model Measurement Based on Digital Close-range Photogrammetry Technique for the Deep Foundation Pit Deformation Monitoring", KSCE Journal of Civil Engineering, 27(2), pp. 577–589, 2023. https://doi.org/10.1007/s12205-022-2045-9

[5] Xu, L., Li, W., Liu, L., Wu, F., Fan, Z., Chen, R. "Deformation analysis of a deep excavation with a servo control system adjacent to an existing foundation pit: A case study in Shenzhen", Tunnelling and Underground Space Technology, 170, 107374, 2026. https://doi.org/10.1016/j.tust.2026.107374

[6] Zhang, W., Heng, C., Xu, C., Zhou, Z., Mao, L. "Research on Support Technology of a Soil-Rock Combination Deep Excavation in Qingdao", KSCE Journal of Civil Engineering, 28(8), pp. 3208–3223, 2024. https://doi.org/10.1007/s12205-024-1067-8

[7] Li, G., Li, Q., Wang, J., Dong, J., Sun, Q. "The Deformation Characteristics of a 40-m-Deep Excavation Supported by a Suspended Diaphragm Wall in Rock and Soil Composite Ground", KSCE Journal of Civil Engineering, 26(3), pp. 1040–1050, 2022. https://doi.org/10.1007/s12205-021-1642-0

[8] Zhou, C., He, L., He, J., Zhang, Y., Xiao, H., Soh, C. K. "Deflection of foundation pit retaining wall in heterogeneous soil strata: Intelligent prediction methods based on physics-informed machine learning", Journal of Rock Mechanics and Geotechnical Engineering, 18(5), pp. 4007–4022, 2026. https://doi.org/10.1016/j.jrmge.2025.07.019

[9] Nicotera, M. V., Russo, G. "Monitoring a deep excavation in pyroclastic soil and soft rock", Tunnelling and Underground Space Technology, 117, 104130, 2021. https://doi.org/10.1016/j.tust.2021.104130

[10] Tabaroei, A., Sarfarazi, V., Pouraminian, M., Danial Mohammadzadeh, S. "Evaluation of Behavior of a Deep Excavation by Three-dimensional Numerical Modeling", Periodica Polytechnica Civil Engineering, 66(2), pp. 501–511, 2022. https://doi.org/10.3311/PPci.20353

[11] Movahedi Rad, M. "Reliability Based Analysis and Optimum Design of Laterally Loaded Piles", Periodica Polytechnica Civil Engineering, 61(3), pp. 491–497, 2017. https://doi.org/10.3311/PPci.8756

[12] Szepesházi, A., Móczár, B. "Two- and Three-dimensional Numerical Back-analysis of Deep Excavation Case Studies from Budapest, Hungary", Periodica Polytechnica Civil Engineering, 67(3), pp. 659–670, 2023. https://doi.org/10.3311/PPci.21829

[13] Movahedi Rad, M., Ibrahim, S. K. "Optimal Plastic Analysis and Design of Pile Foundations Under Reliable Conditions", Periodica Polytechnica Civil Engineering, 65(3), pp. 761–767, 2021. https://doi.org/10.3311/PPci.17402

[14] Atenov, Y., Bekbasarov, I. "Equations Used to Calculate Vertical Bearing Capacity of Driven Piles with Shaft Broadenings", Periodica Polytechnica Civil Engineering, 64(4), pp. 1235–1243, 2020. https://doi.org/10.3311/PPci.16482

[15] Kaveh, A., Hamedani, K. B., Bakhshpoori, T. "Optimal Design of Reinforced Concrete Cantilever Retaining Walls Utilizing Eleven Meta-Heuristic Algorithms: A Comparative Study", Periodica Polytechnica Civil Engineering, 64(1), pp. 156–168, 2020. https://doi.org/10.3311/PPci.15217

[16] Lődör, K., Móczár, B. "Design and Modelling Process of Soil Improvement with Concrete Strengthening Elements", Periodica Polytechnica Civil Engineering, 64(1), pp. 287–295, 2020. https://doi.org/10.3311/PPci.15220

[17] Haouari, H., Bouafia, A. "A Centrifuge Modelling and Finite Element Analysis of Laterally Loaded Single Piles in Sand with Focus on P–Y Curves", Periodica Polytechnica Civil Engineering, 64(4), pp. 1064–1074, 2020. https://doi.org/10.3311/PPci.14472

[18] Vásárhelyi, B., Kovács, D. "Empirical methods of calculating the mechanical parameters of the rock mass", Periodica Polytechnica Civil Engineering, 61(1), pp. 39–50, 2016. https://doi.org/10.3311/PPci.10095

[19] Nie, Q. K., Liang, J. G., Han, L. J., Bai, B. "Design Theory and Application of Double-Row Pile Retaining Structures for Deep Foundation Pits", China Architecture & Building Press, 2008. ISBN 978-7-112-10025-5

[20] Liu, J. H., Hou, X. Y., Liu, G. B., Wang, W. D. "Foundation Pit Engineering Manual", China Architecture & Building Press, 2009. ISBN 978-7-112-11552-5

[21] Gong, X. N., Hou, W. S., Yu, J. L. "Deep Foundation Pit Engineering Design and Construction Manual", China Architecture & Building Press, 2025. ISBN 978-7-112-30356-4